Mechanics of intermittent plasticity punctuated by fracture during shear deformation of Mg alloys at near ambient temperatures

Saurabh Basu[a], Sepideh Abolghasem[a] and M. Ravi Shankar[a,*]

[a]Swanson School of Engineering

3700 O'Hara Street, University of Pittsburgh

Pittsburgh, PA 15261, USA

Microstructure evolution of basal textured Mg alloy AZ31B (Mg: Al: Zn; 96: 3: 1 wt. %) during simple shear deformation at near ambient temperatures was studied by plane-strain machining. Using Schmid factor calculations in conjunction with quantitative electron microscopy, it was found that plastic deformation in AZ31B in the primary deformation zone of machining commences by extension twinning followed by basal slip. Characteristics of twinning in individual grains were described by correlating the direction of twinning with the principal stress state. Implications of these deformation mechanics for the microstructure inherited by the freshly generated surfaces in shear-based material removal processes are examined. These include the identification of extensive surface texture reorientation at machined surfaces via extension twins, limits on surface integrities wrought by fracture events that punctuate plastic deformation and their relationship to the cutting tool geometry.

* Corresponding author: ravishm@pitt.edu

1. Introduction

Magnesium is promising for use in transportation applications wherein its high specific strength may be exploited to manufacture lighter machine elements to achieve step changes in performance and fuel efficiency. Also, Mg alloys have densities similar to that of bones in the human body [1] and the fact that Mg^{2+} is the fourth most abundant cation in humans may offer new frameworks for the fabrication of bioresorbable implants. Despite an array of technological opportunities, the deformation behavior of Mg and its alloys often present challenges to their widespread utilization. The challenges often emerge from its Hexagonally Close Packed (HCP) crystal structure that deforms primarily by twinning and basal slip at room temperature. Its anisotropic nature manifests a high Cross Resolved Shear Stress (CRSS) for non-basal (pyramidal and prismatic) slip [2]. Unlike FCC metals that have five slip systems available to accommodate deformation in any configuration, Mg has only two at room temperature, which results in its characteristic lack of ductility. The resulting poor formability of the material often results in premature fracture during manufacturing operations involving plastic deformation [3].

The discontinuous flow (resulting from premature fracture in chips) in Mg is commonly observed in machining [4], a widely used manufacturing process that is a mainstay of fabrication of metallic components. During the machining process, material being machined undergoes plastic deformation in the fan shaped deformation zone, thereby forming the chip (Figure 1a). Magnesium often lacks the ability to accommodate plastic deformation to form a continuous chip. As a result, the chip formation process is interrupted by fractures that run through the chip near the fan shaped deformation zone. Thereafter as the tool progresses forwards, the chip formation process continues and the aforementioned pattern repeats, due to which the chip 'flow' has been termed discontinuous. Machining is a material removal

process that involves advancing a wedge-shaped tool into a workpiece to remove a pre-set depth of material. Figure 1a illustrates a plane-strain prototype of this process in which the wedge-shaped tool advances in a direction that is normal to the cutting edge. In this fabrication process, sheet material in the regime corresponding to the set depth a_0, is strained in simple shear as it flows through the fan-shaped deformation zone to become the chip. Thickness a_c of the resulting chip depends on material properties of the sheet and the process parameters: V, α (Figure 1a). When the material is deformed by shear, the effective strain accumulated by the material in the chip can be determined as a function of the ratio $\frac{a_0}{a_c}$ and is given by [5]:

$$\varepsilon = \frac{1}{\sqrt{3}} \frac{\cos\alpha}{\sin\varphi\cos(\varphi-\alpha)} \quad (1)$$

where:

$$\tan(\phi) = \frac{a_0/a_c\cos(\alpha)}{1-a_0/a_c\sin(\alpha)} \quad (2)$$

In machining, with $a_c > a_0$ it is common to encounter strains >>1 in ductile metals such as Cu, Al and even some Ti alloys [6-8]. However, Mg is not amenable to such severe plastic deformation at room temperature and manifests a characteristic intermittently deformed/sawtooth chip pattern.

This intermittency of deformation during the chip formation process holds direct implications for the surface integrity of the part generated from machining [9]. It has been shown through *in situ* measurements of the thermomechanics of deformation during machining that the fan-shaped deformation zone (Figure 1a.) extends underneath the tool [8] into the freshly generated surface. Material within this extended deformation zone is deformed as the tool progresses over the workpiece, resulting in altered surface mechanical properties (strength, microstructure, etc.) and surface-nucleated functional properties such as corrosion response

[10]. The spatial contiguity of the deformation zone in machining also results in the microstructural attributes being mirrored between the chip and the freshly-generated surface [11].

The implications of such correlated microstructures between the chip and the surface in the case of Mg would be more complex given that its limited ductility may prevent the imposition of uniform and severe simple shear. Rather, we can anticipate a characteristically discontinuous mechanics of chip formation, wherein segments of plastic deformation are punctuated by fracture. Here, the microstructural implications of deformation in the chip during the plastic deformation pauses would be comparable to that on the freshly generated surfaces. Of course, tool advance that further builds-up plastic strains would lead to abrupt fracture of the chip wherein further uniform shear is no longer possible. Note that the expectations of discontinuity in plastic flow, when attempting to impose severe shear deformation in Mg alloys, are commonly observed [3]. However, elucidation of the microstructural phenomena in the plastic deformation stages between the fracture events under these conditions has been ignored. While such examination is understandably irrelevant when examining bulk deformation, it is critical in manufacturing processes like machining, given that the microstructure on the surface is directly affected by intermittent plastic deformation.

In this study, using electron microscopy, we will examine how the microstructure of a basal texture in wrought Mg alloys evolves by deformation through simple shear during the chip formation process (machining) in the punctuated plastic deformation intervals. We will also elucidate the relevance of this mechanics to microstructure evolution of material under the machining surface in the extended deformation zone. More specifically, we will show that the

AZ31B microstructure evolves by extension twinning and subsequent dislocation generation and storage during simple shear. Furthermore, there is significant texture reorientation by twinning in the material under the surface in the extended deformation zone.

2. Experimental Methods

To accomplish this, we used a 3 mm thick rolled basal-textured sheet of AZ31B (96 wt. % Mg, 3 wt. % Al, 1 wt. % Zn) Mg alloy. The sheet was orthogonally machined in the Rolling Direction (RD parallel to X and TD parallel to Y in Figure 1a.). Through this configuration, the direction of advance of the wedge-shaped tool was kept approximately perpendicular to the c axis of the Mg crystal. This geometric setup is similar to that considered in analogous deformation experiments [12-16], wherein the direction of applied stress is maintained perpendicular to the c axis of Mg. Note that this is also the orientation in which typically basal textured sheet forms of Mg would likely be subjected to metal cutting in processes such as milling, drilling, etc. during sheet-metal part fabrication.

A freshly sharpened (< 5 μm edge radius) High Speed Steel (HSS) wedge-shaped tool ($\alpha = 40^o$) was advanced against a preset depth (a_0) of 100 μm at a speed (V) of 2 mm/s (Figure 1a.). It is known that machining involves coupled thermomechanics and the speed V directly influences the temperature in the deformation zone [17]. In machining of Mg this is a critical concern because of the fire hazards associated with ribbon like Mg chips due to high flammability and low auto-ignition temperature (~473 ˚C). Here, in seeking to establish a baseline for understanding the microstructural implications of chip formation, we have chosen a small value for V to examine thermal conditions close to ambient. This was confirmed by measuring the temperature *in situ* in the deformation zone using calibrated InfraRed (IR) thermography that was performed by observing the deformation zone using a

FLIR infrared camera. The information obtained from the camera (counts) was converted to temperature using a preset calibration curve [6]. The calibration procedure involved coating a metallic plate with a suitable black paint and then heating the plate to temperatures between near ambient to 300 ˚C and subsequently observing through the FLIR infrared camera. Here, coating the plate with the black paint ensured an emissivity of close to one. Eventually, a calibration curve was constructed by correlating the data (counts) obtained from these observations with the corresponding temperatures. Finally, while performing infrared thermography of the deformation zone of Mg alloy during machining, the side of the workpiece was also coated with the same black paint to ensure similar emissivity and the temperature field was calculated point-by-point using the calibration curve.

For optical metallography of the deformation zone, partially detached chip specimens were created and mounted in epoxy. Thereafter, the specimens were mechanically polished down to a 0.05 μm alumina finish and etched by dipping in acetic picral (5 mL acetic acid, 6 g picric acid, 10 mL water, 100 mL ethanol) for ~10 seconds. Supplementing optical characterization, Orientation Image Mapping (OIM) of the microstructure in the deformation zone leading into the chip was performed using Electron Back Scattered Diffraction (EBSD) in a JEOL JSM 6610LV scanning electron microscope equipped with an HKL Technologies Nordlys EBSD detector. Specimens were created by mechanically polishing epoxy-mounted and partially detached chip samples, followed by electro-polishing using a solution of 30 vol. % Nitric Acid, 70 vol. % Ethanol at a temperature of -30˚C at a potential difference of 12 V. Directional [0002] texture on the surfaces created by machining was measured using a Philips PW1830 X Ray Diffractometer. This was done by using a ϕ step size of 5˚ at a time per step of 3 s and Ψ step size of 5˚ degrees. Initially, texture measurements were performed on the surface created by the $\alpha = 40^{o}$ tool. Subsequently, to identify the effect of tool geometry on

texture reorientation, texture measurements were also performed on a surface created by an $\alpha = -20^{o}$ tool.

3. Results

3.1 Strain and Temperature in the primary deformation zone

The effective strain imparted by the advancing tool to the material that forms the chip was measured empirically. This was done by measuring the ratio $\frac{a_0}{a_c}$ whereby $\tan(\phi)$ (Eqn. 2) was determined ($\alpha = 40^{o}$). Subsequently, equation (1) was used to calculate the value of effective strain $\varepsilon = 0.52$.Temperature in the deformation zone was measured using IR thermography using the procedure described. This is illustrated in Figure 1b and shows a moderate temperature rise of approximately 10˚ C in the primary deformation zone. Complicating effects of deformation mechanisms other than twinning and basal slip can therefore be safely disregarded from the analysis.

3.2 Optical Microscopy of deformation zone

Microstructure in the deformation zone was exposed by polishing and etching using the procedure described. Figure 2 shows the evolution of bulk microstructure across the deformation zone observed by optical microscopy as it flows to form the chip. The sample that was used to make Figure 2 was generated by performing a quick stop experiment while machining the Mg alloy sheet. In this manner the chip was left attached to the sheet work piece. This was done on purpose so that the gradation in microstructure from the workpiece to the chip, as revealed by optical and electron microscopy could be studied. The sample was not quenched thereafter. This was because the negligible rise in temperature in the deformation zone of the sample (as observed by IR thermography) was not expected to cause changes to the microstructure. This sample was thereafter mounted in epoxy and

progressively polished to a 0.05 μm alumina finish. Thereafter, the exposed polished metal surface was etched with acetic picral for ~ 10 s until it acquired a brownish tinge. The etchant was then quickly washed away with ethanol and very briefly with water which was immediately dried off with a blast of air. Note that the bulk microstructure has a much smaller density of intragranular defects and therefore exhibits lower average local image contrast through bright field microscopy, in comparison to the chip microstructure that exhibits higher average local image contrast. This is attributable to significantly higher densities of microstructural defects in the chip that are prone to rapid etching. This change in concentration of contrasting features was quantified by calculating the localized Root Mean Squared Contrast (RMSC) [18] in the bright field microscopy image whereby an average chip RMSC value of 26.2 was obtained, approximately four times the average intragranular bulk RMSC value 7.3. Obviously, this increase in the defect concentration was caused by imposition of strain during machining. We see that as material flows along the trajectory A-B-C, it shows the first incidence of twinning at around B that is closer to the edge of the fan shaped deformation zone DEF where material starts deforming. This is indicated using black arrows in Figure 2. It is known that twinning precedes other deformation modes during deformation in basal-textured Mg alloys [13]. Using this fact, it is reasonable to assume that this spatial region (interspersed with twins) marks the edge of the primary deformation zone where material begins to deform. Note that the twinned lamellae features are etched to a much higher extent than the surrounding grain during the etching process and appear darker when observed through a light microscope. A similar exhibition of high contrast twins was observed during analogous experiments on deformed Mg where reorientation induced increase in interatomic planar distances amplified the etching rates [10]. However, it will also be seen that the twinned regions within the grains are more susceptible to deformation by dislocation multiplication and storage. The contrast within twin lamellae in the bright field

microscopy images revealed by relatively higher etching rates may therefore be attributable to a combined effect of increased defect densities as well as interatomic spacing. Beyond this twin-dominated region, material also deforms by dislocation multiplication and storage, as is evident from the increasing density of contrasting features that results in a dense metallographic feature-rich zone covering the entire region closer to C [8]. Quantitative evidence in support of this argument is given in the discussion section.

3.3 Quantitative electron microscopy by Orientation Image Mapping (OIM) using Electron Back Scattered Diffraction (EBSD)

Figure 3 shows the results of OIM of the microstructure in the deformation zone leading into the chip, performed using EBSD. Inset (a) shows the Image Quality (IQ) map obtained from EBSD. Twins are overlaid in the IQ map with yellow lines for the {1 0 -1 2} <-1 0 1 1> extension twinning mode, representing a measured misorientation of 86 $\pm$ 5˚. We observe that the microstructure consists of interspersed extension twins, with the density of twins increasing closer to the chip in the deformation zone. Note from the IPF color index (blue) that these extension twins are oriented with non-basal planes parallel to the side surface along the orientation of observation in Figure 2 and therefore stand out in stark relief versus the neighboring grains during etching [10] (refer to inset b in Figure 3 showing corresponding IPF coloring). Dislocation activity starts after twinning, as suggested by low Kikuchi band slope further into the chip, as we progress away from the twinned regions. A high average band slope of approximately 119 was found for grains in the bulk as opposed to a low value of 67 for grains in chips where the detection of Kikuchi bands by EBSD was possible. Note that the density of ‘extension’ twins increases closer to the chip in the deformation zone, indicating that incremental deformation in the initial stages of chip formation is accommodated by this mode (extension) of twinning. This is similar to the observed mode of

twinning in compression experiments [13, 19] where the compression axis is parallel to Rolling Direction (RD), implying perpendicularity with the c axis of Mg.

3.4 [0002] texture on the surface created by machining

Figure 4a. shows the [0002] pole figure obtained by texture measurements on the side as-received rolled sample, confirming a predominantly basal texture. This is also confirmed by the absence of diffracted intensity of the [0002] peak of Mg near the periphery (Figure 4a), which implies that the majority of grains in the sheet-shaped sample can be assumed to be oriented with their c axes normal to the plane of the sheet (c axis normal to XY plane, i.e. along the Z plane in Figure 1a). This is in contrast with the [0002] pole figures obtained from texture measurements from the fresh surface created by machining with $\alpha = 40^{o}$ tool (Figure 4b), i.e. along the XZ plane. This suggests higher concentration grains with c axis oriented towards sample reference X axis (in Figure 1a). Texture measurements from the freshly generated surfaces created with the $\alpha = -20^{o}$ tool were also performed and the results are illustrated in Figure 4c. It is clear from the similar patterns of [0002] pole figures obtained from the two machined surfaces that deformation of material in the surface during machining results in reorientation of the basal texture. However, the increase in intensities of [0002] texture for $\alpha = -20^{o}$ suggests a variation that was caused by changing the tool angle α, which in turn controls the deformation strain [5]. Here, the more severe shear strains that are imposed by the more negative rake angle tool intensify the reorientation of the basal planes to an orientation that is at an angle of approximately $23.8°$ to the machined surface. It would therefore be justified to say that machining causes significant texture reorientations on the freshly-created surface, an effect that can be controlled by varying tool geometries.

4. Discussion

The following section provides insights into origins of the preferred (extension) twinning mode observed in machining. Microstructural evolution here takes a similar course as in some compression-based deformation experiments on AZ31 B polycrystals, suggesting relatable deformation states between their deformation geometries. An extension of insights drawn from such observations is used to explain microstructure evolution near the surface.

4.1 Twinning mode

The two most commonly observed twinning modes in Mg are the extension and contraction twinning, referring to the extension/contraction of the Mg crystal along its c axis. More specifically, it has been seen in compression deformation experiments (where the principal stress direction is perpendicular to the c axis) that Mg prefers to twin in the extension mode [13]. Similar twinning behavior in the deformation zone of machining indicates some similarities that exist in their stress states in spite of enormously different deformation geometries. As these similarities are likely to yield comparable microstructural responses, insights drawn from these observations would be directly applicable to analysis of material evolution in the deformation zone under the tool, where a stress state similar to the primary deformation zone is known to exist.

Consider the free body diagram of the chip created while machining a basal textured Mg alloy sheet (Figure 5a), showing forces due to the tool and the workpiece. The force between the workpiece and the chip is denoted $\vec{R}$ and between the tool and the chip $\overrightarrow{R'}$. Under equilibrium, these are the same ($\vec{R} = -\overrightarrow{R'}$). These forces may be resolved in the following manner:

1. In the horizontal and the vertical direction (Fp and Fq, respectively)

2. Along the tool face and perpendicular to the tool face (Fc and Nc, respectively)

3. Along and perpendicular to the shear plane (Fs and Ns)

Any of these coordinate systems might be chosen to represent the stress state. Arbitrarily choosing the shear plane coordinate system (3), the stress state in the shear plane may be represented as:

$$\sigma = \begin{matrix} -Ns/A & -Fs/A & 0 \\ -Fs/A & 0 & 0 \\ 0 & 0 & 0 \end{matrix} \quad (3)$$

where A is the area of the shear plane. Here $-Fs/A$ is the mean shear stress acting on the shear plane [5] due to the workpiece.

Now consider the free body diagram showing compression perpendicular to the c axis of Mg as shown in Figure 5b. Stress state in plane strain compression in the sample coordinate system is given by $\sigma = \begin{matrix} -F/A & 0 & 0 \\ 0 & 0 & 0 \\ 0 & 0 & 0 \end{matrix}$

where A is the cross sectional area of the sample.

Rotating this to the crystal coordinate system for the case of basal textured sheet,

$$\sigma = \begin{bmatrix} \cos\theta & -\sin\theta & 0 \\ \sin\theta & \cos\theta & 0 \\ 0 & 0 & 1 \end{bmatrix} \begin{bmatrix} \frac{-F}{A} & 0 & 0 \\ 0 & 0 & 0 \\ 0 & 0 & 0 \end{bmatrix} \begin{bmatrix} \cos\theta & \sin\theta & 0 \\ -\sin\theta & \cos\theta & 0 \\ 0 & 0 & 1 \end{bmatrix} =$$

$$\therefore \sigma = \begin{matrix} -\cos^2\theta\, F/A & -\cos\theta\sin\theta\, F/A & 0 \\ -\cos\theta\sin\theta\, F/A & 0 & 0 \\ 0 & 0 & 0 \end{matrix} \quad (4)$$

Here θ is the orientation of the crystal with respect to the loading direction. Note that $\theta \in [0, 90^\circ]$ due to the symmetry of the HCP crystal structure. This implies that σ_{11} and σ_{12} will remain –ve as in (3).

This shows how the deformation and stress states of the primary shear zone in machining and of compression tests are quite relatable, wherein the principal stress direction is perpendicular

to the c axis. An extension of the same idea can be employed to predict the chosen directions of twinning during simple shear deformation, due to the prevalent localized stress states in different grains. For example, extension twinning involves shear in the {1 0 -1 2} plane along the <-1 0 1 1> direction and causes a rotation of 86.3˚ of the c axis about the <-12-10> axis [14]. This is shown in Figure 3d (adapted from [20]). Owing to the six fold crystallographic symmetry of the Mg crystal, there are six ways of choosing these twin systems (involving shear plane, shear direction and rotation axis). Any dependence of the chosen twinning mode on the localized stress state must therefore also be reflected on the resulting twinning system. The direction of principal shear stress (as it directly influences the localized stress state) acting on the different grain-twin pairs was superimposed on their crystallographic orientation for understanding the reorientations caused by twinning (Figure 3). This was done for twins marked by arrows I and II in region 1, III and IV in region 2 and V in region 3 of Figure 3. The principal shear stress direction (shown in Figure 3c) was manually calculated by inspection of the chip sample on which OIM was performed. By comparing initial and twinned orientations, we observe a similar (and expected from the direction of principal shear stress) reorientation in at least four of the representative twinning incidents chosen from Figure 3 (Figure 3-I, 3-II, 3-III, 3-IV). The aforementioned expected direction of reorientation corresponds to the twinning mode (one of the six {10-12} <10-11> extension twinning systems) for which direction η_1 (by the Bilby and Crocker [21] notation) was closest to the principal shear stress direction in the orthogonal machining experiment performed here. This was however not true in case of Figure 3-V where the grain seems to have reoriented perpendicularly with respect to the direction of principal shear stress (expected reorientation shown in red). A possible explanation of this observation may be obtained from the spatial location of the parent grain that undergoes this twinning. The grain is located close to the tool face and is influenced by the secondary deformation field (shear),

caused by friction forces acting along the face of the tool against the flow of the chip (Figure 3c). Here, the direction of shear stress that reorients this grain by twinning is different from that expected from the simple shear configuration prevailing elsewhere in the chip, away from the frictional boundary. In fact, we see that if this direction is made parallel to the face of the tool (white arrow in Figure 3-V), the direction in which the frictional force acts, then the reorientation is quite reasonable. This clearly shows that the chosen direction of twinning in a grain is highly influenced by the prevalent local stress state, specifically the principal stress direction within the grain. This fact goes on to reinforce our arguments in the previous paragraph that incidences of "extension" twinning may be attributed to the stress state. One may also deduce from this observation, in conjunction with the spatial contiguity of the deformation zone, that material closer to the tool under the surface created by machining must also respond similarly (by extension twinning), owing to comparable stress states in the chip ahead of the tool and region underneath the tool. This must therefore result in textural reorientation of the material closer to the surface, which is created by machining and this has been discussed in the next section.

4.2 Reorientation of texture of the material under the surface created by machining

It was demonstrated in section 3.4 that there is significant texture reorientation of the material under the surface that is created during machining. Furthermore, the extent of this reorientation was shown to depend on tool angle α. While it is well known that reorientation can be caused by dislocation slip, the limited levels of plastic strains that are permissible in Mg, in conjunction with the observed extensive magnitude of reorientations (from predominantly non basal to basal), preclude this possibility. This hints at twinning due to deformation caused by the progressing tool as the reason behind such reorientation.

Texture reorientation in Mg during cold [22] as well as mildly hot [23] (~200 ˚C) shear

deformation processes has been commonly observed. Consequences of such events include a 'shift' in yield anisotropy whereby some orientations become very ductile while others do not. Obviously, from a forming operation perspective, necessitating isotropic yield behavior, the aforementioned is a point of concern. It has been seen that a weaker (more random) texture is instrumental in reducing strain anisotropy during forming operation, albeit at mildly hot temperatures (150 ˚C) [24]. However, from a machining perspective, textural reorientation in material under the surface can be considered as an opportunity to exploit orientation-dependent functional properties [10].

Optical metallography (Figure 6b) shows that the material under the surface created by machining is interspersed with twins. This suggests that a similar stress state as the one existing in the primary deformation zone is prevalent in the material under the progressing tool during machining. We also saw in section 4.1 that such a stress state can be resolved from a purely compressive stress state by rigid body rotation of coordinate axes, suggesting a compressive stress state existing in the material under the progressing tool. In fact, this observation goes hand in hand with the preexisting knowledge of compressive stress states existing underneath the tool in machining [25], reinforcing our arguments. Note the much deeper extensive region under the surface that has undergone twinning when machining with $\alpha = -20^{o}$ tool (Figure 6c). This phenomenon is directly reflected on the increased intensity of the [0002] texture on the surface (~1373 for $\alpha = -20^{o}$and ~650 for $\alpha = 40^{o}$). At first glance, the extended twinning region for $\alpha = -20^{o}$ as compared to $\alpha = 40^{o}$ appears to be a result of higher deformation imparted with a more negatively angled tool. However, there is some evidence about the positive influence of hydrostatic pressure on inclination for twinning during deformation [26]. Therefore, the extended twinning region might also be attributed to the increased compressive hydrostatic stresses that are caused in the subsurface of the bulk material when traversed by the more negative tool ($\alpha = -20^{o}$). Furthermore, it must be noted

that although the discussion provided in the section is based on results obtained from multiple measurements in each case, it represents two data points only ($\alpha = -20^o, 40^o$). Observations from several samples were made for optical microscopy and four samples for electron microscopy before results were summarized. Results presented include the samples that typify the microstructural transformations outlined in the paper. Quantitative data supporting our arguments (Kikuchi band slope and local image contrast) were obtained from the images presented in the manuscript, albeit from large areas within them whereby they can be termed statistically significant. More work is ongoing to resolve this.

4.3 Deformation by slip following twinning

The Schmid Factors (SF) for extension twinning and basal slip were calculated for the machining geometry under consideration. Areas in the corresponding SF maps near the twinned regions are shown in insets 'T' and 'B' in Figure 3, referring to twinning and basal slip, respectively. The three zones considered have been labeled 1, 2 and 3 and their twinning and basal slip SF insets shall be referenced as T1, T3, B1, etc. We observe a characteristic increase in SF for basal slip in most of the twin lamellae when compared to the area of the grain surrounding the twin. This increase in SF must have been affected by the change in orientation caused by twinning. However, we also note that this increase in SF for basal slip was not always accompanied by any intuitively similar trend of decrease in SF for twinning. In fact, some extension twinned regions showed an increase in the extension twin SF after grain reorientation caused by twinning (refer B2, T2 in Figure 3). It is important to note at this stage that CRSS for basal slip is smaller than CRSS for twinning [15]. This implies that after sufficient rise in SF induced by reorientation due to twinning, basal slip is likely to take over as the primary deformation mode even though twinning may have a higher SF in the present configuration [16, 27]. These insights suggest that after reorientation caused by

twinning, highly concentrated deformation by basal slip ensues in the twinned regions, leading to failure after a small increment in strain. Note that similar observations have been reported in literature during plane strain deformation [13, 14]. Failure is punctuated as a crack that runs through the chip such that the entire process restarts, resulting in sawtooth chip formation.

Figure 6a shows a section of a chip obtained from machining AZ31 with $\alpha = 40^{\circ}$ at low speed. This section was chosen for ease of illustration and is representative of the phenomena at play in the primary deformation zone of machining from which the chip originates. The discussion presented in this section was verified by generation and subsequent etching treatments and optical microscopy imaging of many chips, all of which resulted in similar microstructural features. Note the conserved grain boundary features in the chip (pointed using white arrows in Figure 4a; black arrows show twins within those grains) surrounding grains of size ~ 10 - 20μm, similar to bulk microstructure (Figure 2). This lack of grain refinement suggests that severe plastic deformation that otherwise occurs in more ductile materials does not happen here and is further symptomatic of the discontinuous mechanics of plastic deformation during chip formation. Figure 6b shows the surface topography that was obtained from the same experiment. The surface is wavy and irregular and is directly related to the discontinuous mechanics associated with the sawtooth chip formation, where material removal by plastic deformation is punctuated by events of fracture that bequeath an uneven freshly generated surface. Often on machined surfaces, such poor finishes and uneven topographies are undesirable due to their effect on an array of functional, as well as mechanical properties such as fatigue life [28].

5. Conclusions

Microstructural evolution of basal textured AZ31B during deformation by simple shear at near ambient temperatures is described. For this, orthogonal machining was performed on

textured AZ31B sheets at a low speed with the direction of machining parallel to the rolling direction of the sheet, making the deformation approximately perpendicular to the c axis of Mg crystal. Deformation commences in the fan-shaped zone of machining by extension twinning. Reorientation caused by twinning depends on the local deformation state of the parent grain and leads to subsequent basal slip in the twinned lamellae. This is evidenced from an increase in the Schmid Factor for basal slip in these twinned lamellae. However, many grains with pristine grain boundaries and of similar sizes as in the bulk were observed in the chip through optical microscopy. This deformation behavior featuring twinning induced basal slip is also observed in some compression experiments where the axis of compression is parallel to the rolling direction of the sample, despite contrasting process geometries between compression experiments and machining. Reasons for this were described through congruence in their deformation states that resulted in relatable microstructural consequences. The microstructure closest to the freshly generated surface created during machining also shows a presence of twins. This is because of the spatial contiguity of the new surface with the deformation zone whereby the surface inherits similar microstructural features as the chip. It was deduced that twinning in the material under the surface was also caused by a similar geometrical stress state there as that present in the primary deformation zone of machining. This results in significant texture reorientation, resulting in a predominantly basal texture normal to the surface. Intermittent fracture disrupts material flow that endows an irregular surface topography on the machined surface.

Acknowledgement

Support from the National Science Foundation (CMMI grant #0856626) is gratefully acknowledged.

6. References

[1] F. Witte, J. Fischer, J. Nellesen, H.A. Crostack, V. Kaese, A. Pisch, F. Beckmann., H. Windhagen: Biomaterials, 2006, vol. 27, pp. 1013–1018.
[2] J. Koike, T. Kobayashi, T. Mukai, H. Watanabe, M. Suzuki, K. Maruyama, K. Higashi: Acta Mater., 2003, vol. 51, pp. 2055-2065.
[3] F. Kang, J.T. Wang, Y. Peng: Mat. Sci. Eng., A, 2008, vol. 487, pp. 68-73.
[4] H.T. Friedrich, B.L. Mordike: Magnesium Technology - Metallurgy, Design Data, Applications, Springer-Verlag, Germany, 2006.
[5] M.C. Shaw: Metal Cutting Principles, Oxford University Press, Inc., New York, 2005.
[6] S. Abolghasem, S. Basu, S. Shekhar, J. Cai, M.R. Shankar: Acta Mater., 2012, vol. 60, pp. 376-386.
[7] M.R. Shankar, S. Chandrasekar, W.D. Compton, A.H. King: Mat. Sci. Eng., A, 2005, vol. 410–411, pp. 364–368.
[8] M.R. Shankar, B.C. Rao, S. Lee, S. Chandrasekar, A.H. King, W.D. Compton: Acta Mater., 2006, vol. 54, pp. 3691-3700.
[9] A.A. Lipatov: Russian Engineering Research, 2008, vol. 28, pp. 904-905.
[10] Z. Pu, S. Yang, G.L. Song, O.W.D. Jr., D.A. Puleo, I.S. Jawahir: Scr. Mater., 2011, vol. 65, pp. 520-523.
[11] R. Calistes, S. Swaminathan, T.G. Murthy, C. Huang, C. Saldana, M.R. Shankar, S. Chandrasekar: Scr. Mater., 2009, vol. 60, pp. 17-20.
[12] A. Jain, O. Duygulu, D.W. Brown, C.N. Tom´e, S.R. Agnew: Mater. Sci. Eng. A, 2008, vol. 486, pp. 545-555.
[13] H. Yang, S. Yin, C. Huang, Z. Zhang, S. Wu, S. Li, Y. Liu: Adv. Eng. Mater., 2008, vol. 10, pp. 955-960.
[14] M.D. Nave, M.R. Barnett: Scr. Mater., 2004, vol. 51, pp. 881-885.
[15] C.J. Boehlert, Z. Chen, I.G. Urrutia, J. Llorca, M.T.P. Prado: Acta Mater., 2012, vol. 60, pp. 1889-1904.
[16] S.G. Hong, S.H. Park, C.S. Lee: Acta Mater., 2010, vol. 58, pp. 5873-5885.
[17] C. Huang, T.G. Murthy, M.R. Shankar, R.M. Saoubi, S. Chandrasekar: Scr. Mater., 2008, vol. 58, pp. 663-666.
[18] E. Peli: J. Opt. Soc. Am. A, 1990, vol. 7, pp. 2032-2042.
[19] S. Godet, L. Jiang, A.A. Luo, J.J. Jonas: Scr. Mater., 2006, vol. 55, pp. 1055-1058.
[20] E. Tenckhoff: ASTM Spec. Tech. Publ. (STP), 1988, vol. 966, pp.
[21] B.A. Bilby, A.G. Crocker: Proc. R. Soc. A, 1965, vol. 288, pp. 240-255.
[22] M.R. Barnett, M.D. Nave, C.J. Bettles: Mater. Sci. Eng., A, 2004, vol. 386, pp. 205-211.
[23] S.R. Agnew, J.A. Horton, T.M. Lillo, D.W. Brown: Scr. Mater., 2004, vol. 50, pp. 377-381.
[24] C.E. Dreyer, W.V. Chiu, R.H. Wagoner, S.R. Agnew: J. Mater. Process. Technol., 2010, vol. 210, pp. 37-47.
[25] C. Wiesner: Metall. Mater. Trans. A, 1992, vol. 23, pp. 989-996.
[26] R.A. Lebensohn, C.N. Tom´e: Philos. Mag. A, 1993, vol. 67, pp. 187-206.
[27] S. Gollapudi, M.A. Azeem, A. Tewari, U. Ramamurty: Scr. Mater., 2011, vol. 64, pp. 189-192.
[28] S.K. As, B. Skallerud, B.W. Tveiten, B. Holme: Int. J. Fatigue, 2005, vol. 27, pp. 1590–1596.

Figure 1. (a) Schematic showing fan shaped deformation zone in orthogonal machining. (b) Temperature field in deformation zone measured by infra-red thermography showing moderate temperature rise during machining (α=40˚, V=2mm/s).

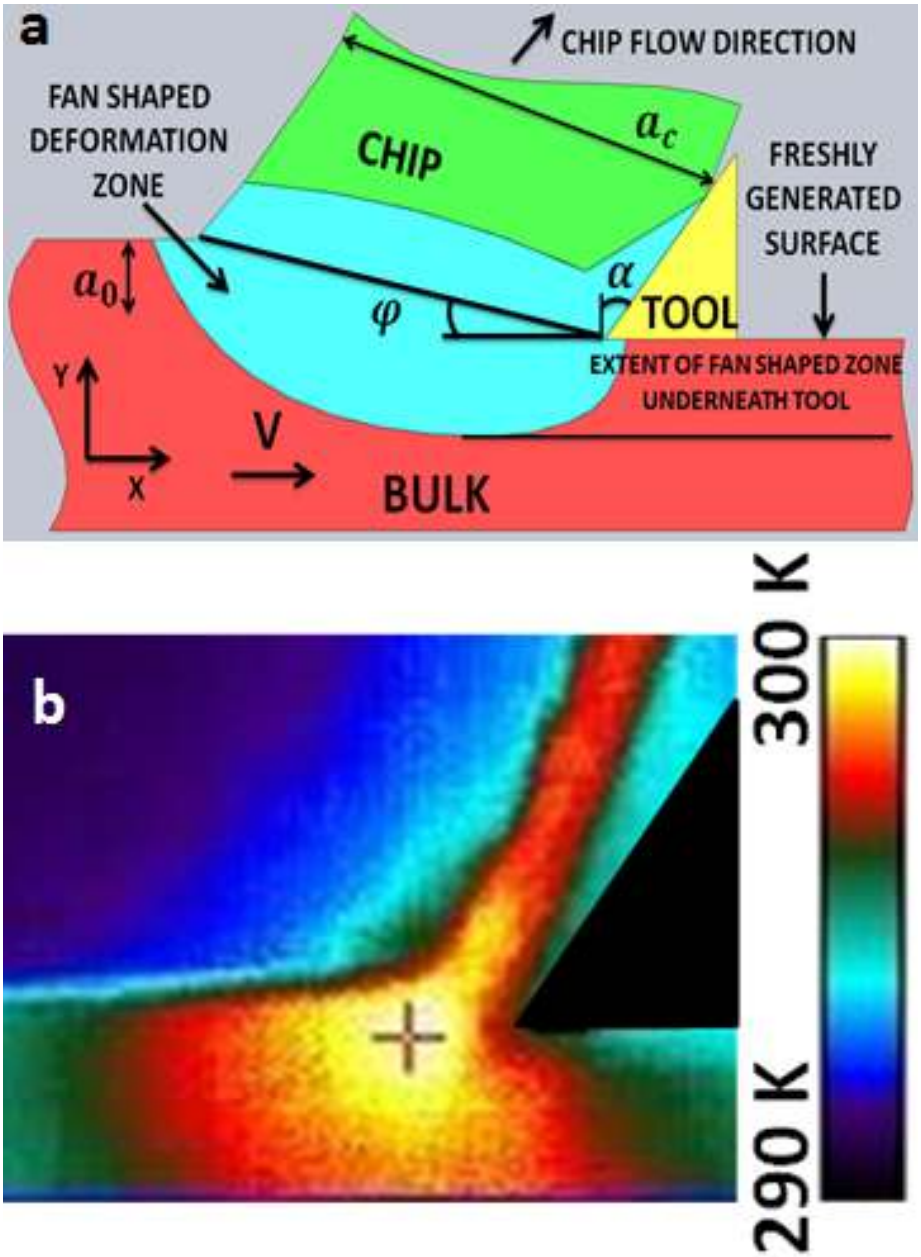

Figure 2. Optical microscopy of the metallographic structure showing evolution of microstructure of workpiece machined with (α=40˚, V=2mm/s) tool as it flows to form the chip. Serrated cracks in the chip are indicated with white arrows. Twins are pointed with black arrows. ABC is a representative path line and DEF is the edge of the fan shaped deformation zone.

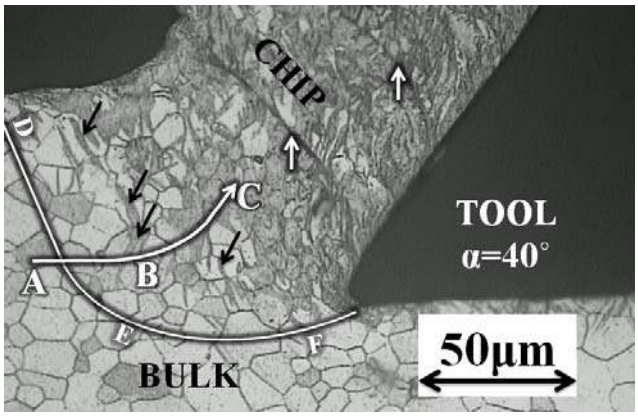

Figure 3. Microstructure evolution of AZ31 B in the deformation zone of machining obtained using EBSD. (a) Image Quality Map showing extension twins (yellow) (b) Inverse pole figure (crystallographic orientation may be obtained from inset). (c) Direction of principal shear stress and secondary shear zone. (d) Change in orientation of the Mg HCP crystal by extension twinning. I, II, III, IV and V show the observed change in orientation due to extension twinning of grains highlighted within insets 1, 2 and 3. Schmid factor for extension twinning (marked T) and Basal slip (marked B) for selected parts of the microstructure map are also shown in 1, 2 and 3.

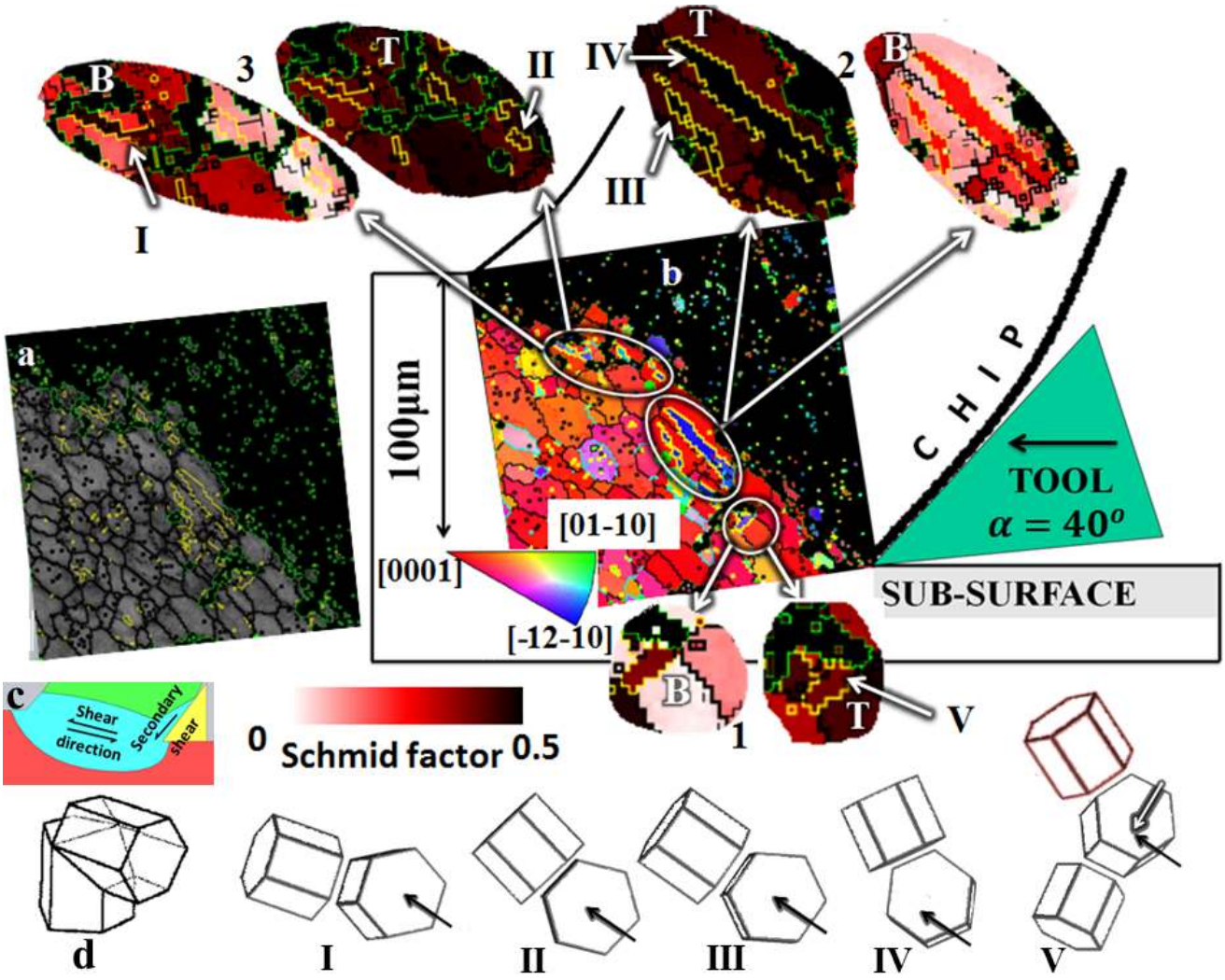

Figure 4. [0002] textures obtained from (a) Side surface of the sheet shaped workpiece. (b) Surface created by the $\alpha = 40^{o}$ tool. (c) Surface created by the $\alpha = -20^{o}$ tool. Refer scales for min and maximum intensities of [0002] textures measured. White arrow shows reorientation of caused by machining. The inset below shows the direction of orthogonal machining (black arrow) and respective positions on the workpiece from where [0002] textures were measured.

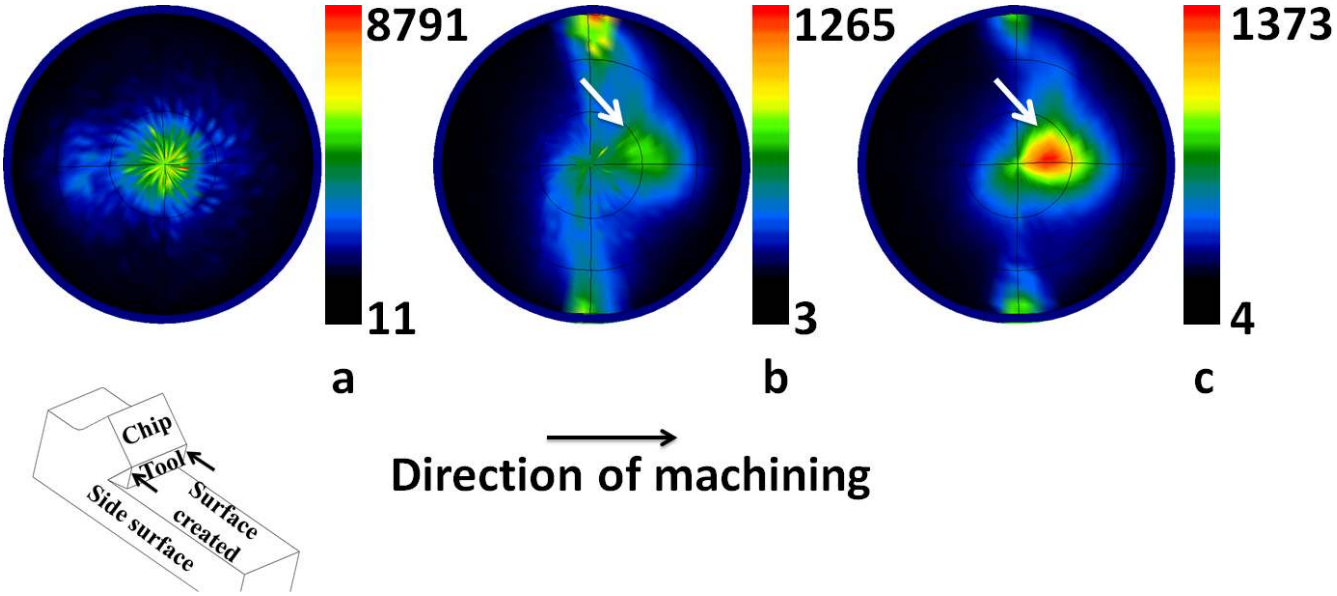

Figure 5. (a) Free body diagram of a chip with chip coordinate system. (b) Illustration of compression of basal texture AZ31 B sheet in the rolling direction (sample coordinate system shown)

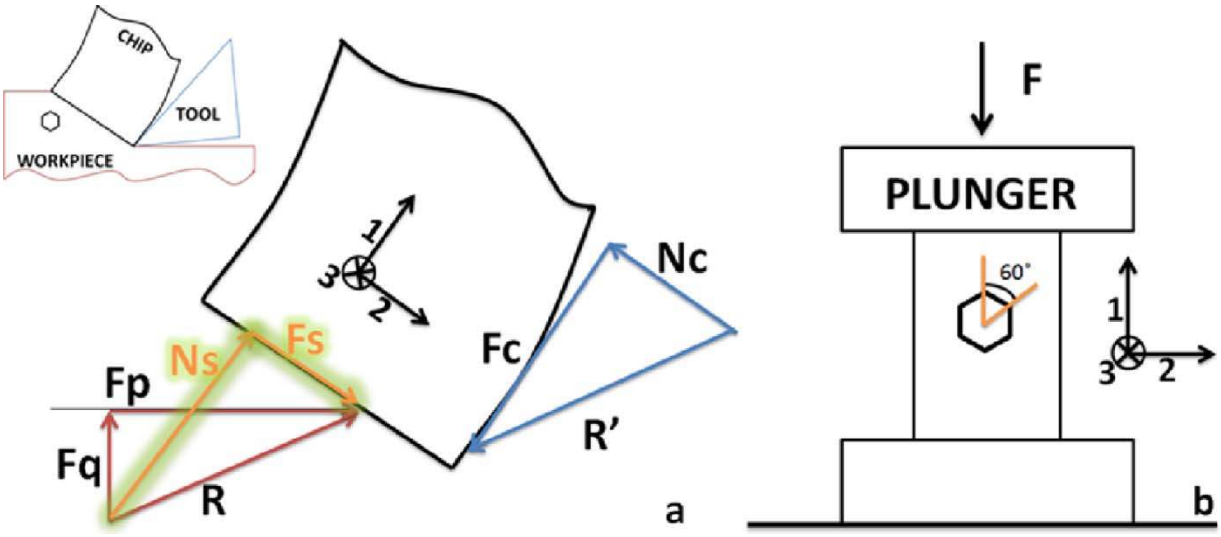

Figure 6. Etched microstructures in the chip and surface obtained by light microscopy. (a) Etched microstructure of chip obtained from machining AZ31 with α = 40˚ at V=2mm/s. White arrows show pristine grain boundaries of unrefined grains indicating incomplete deformation. Black arrows show twin lamellae within these grains. (b) Representative surface topography from the side resulting from machining with α =40˚at V=2mm/s showing wavy surface obtained due to discontinuous flow during material removal where fracture interrupts shear deformation.